Available online at www.sciencedirect.com
SCIENCE DIRECT
Polymer 47 (2006) 6172–6186
polymer
www.elsevier.com/locate/polymer

Microstructural features, diffusion and molecular relaxations in polyimide/silica hybrids

Pellegrino Musto [a,*], Mario Abbate [a], Marino Lavorgna [b], Giuseppe Ragosta [a], Gennaro Scarinzi [a]

[a] *Institute of Chemistry and Technology of Polymers (ICTP), National Research Council of Italy, Via Campi Flegrei 34, Olivetti Building, 80078 Pozzuoli, Naples, Italy*
[b] *Institute of Composite and Biomedical Materials, National Research Council of Italy, P.le Tecchio, 80, 80125, Naples, Italy*

Received 6 February 2006; received in revised form 29 May 2006; accepted 30 May 2006
Available online 12 July 2006

Abstract

FTIR spectroscopy has been used to investigate the microstructure of the inorganic phase in polyimide/silica hybrids obtained by the sol–gel route. It has been shown that the presence of a coupling agent (GOTMS) strongly influences the silica phase by favoring the formation of linear, branched chains which make the structure loosely interconnected. The morphological changes induced by GOTMS are reflected in the water sorption properties of the investigated systems. Due to the hydrophilic nature of the silica phase, the amount of sorbed water increases in the hybrid systems in comparison to the pristine polyimide, and among the two hybrids, increases more in the two-phase system than in the co-continuous. Molecular interactions of the hydrogen-bonding type have been identified between the imide units and the H_2O molecules, both in the polyimide and in the hybrid systems. Finally, the sub-T_g relaxation processes have been investigated in detail by dynamic-mechanical analysis coupled with molecular mechanics simulations. Considerable effects of the inorganic phase on these processes were observed, especially for the case of the co-continuous systems, and were accounted for by molecular scale contiguity among the phases.

Keywords: Nanocomposites; Hybrids; Polyimide

1. Introduction

Organic–inorganic (O/I) hybrid materials prepared by the sol–gel route have emerged as one of the most promising research areas in material science. These systems exhibit the advantageous properties of organic polymers (i.e. ductility, processability), coupled with those of the inorganic components (rigidity, low thermal expansion, inertness) and have been successfully employed in advanced applications such as lenses, waveguide materials, nonlinear optical materials, semiconductors, membranes [1–4].

It turns out that the sol–gel process represents a very versatile method for the preparation of such materials and for the control of their morphology. The sol–gel route can be viewed as a two-step network forming process, the first step being the hydrolysis of a metal alkoxide catalysed by acidic or basic initiators (typically diluted HCl) and the second consisting of a condensation reaction [5,6]. The chemistry of the sol–gel process can be summarized as in Scheme 1.

Often a further component is added to the reactive mixture in order to improve the interaction of the silica glass to various substrates. Typically, it has a structure similar to that of TEOS, with one arm bearing a reactive functional group. In the

* Corresponding author. Tel.: +39 081 8675202; fax: +39 081 8675230.
E-mail address: musto@ictp.cnr.it (P. Musto).

0032-3861/$ - see front matter © 2006 Elsevier Ltd. All rights reserved.
doi:10.1016/j.polymer.2006.05.074

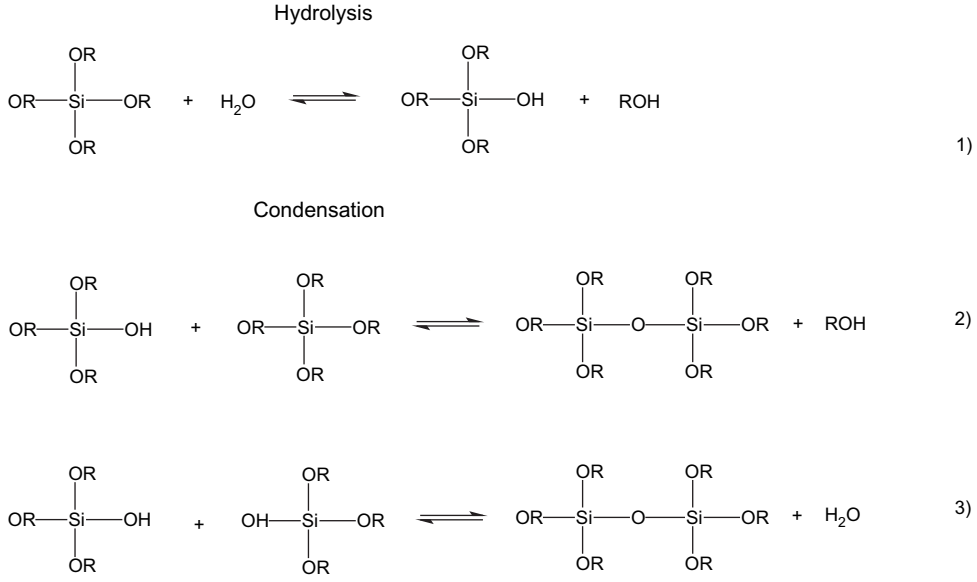

Scheme 1.

present case, γ-glycidyloxypropyltrimethoxysilane (GOTMS) is used, whose structure is reported below:

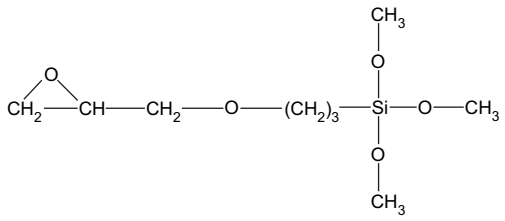

The epoxy end-group is intended to react with the substrate, thus anchoring the silica phase onto it, but, if this reaction does not occur, the epoxy group can, at suitably high temperatures, react with silanol moieties, resulting in the permanent incorporation of $-CH_2-CHOH-CH_2-$ groups into the otherwise inorganic network. This will perturb the regularity of the silica structure.

Polyimides are among the few polymer matrices suitable for the production of O/I hybrids, as they can be obtained from a polyamic acid precursor, which is soluble in hygroscopic solvents and can tolerate the addition of water necessary to bring about the hydrolysis of the alkoxide. Moreover, since the imidization reaction for the conversion of a polyamic acid to the corresponding polyimide is an intramolecular process, it is not adversely affected by the surrounding inorganic domains. At the same time, the excellent thermal stability of polyimides makes it possible to use high temperatures for the development of the silica network (up to 350 °C) without inducing appreciable degradation of the organic phase [2–4].

It has been demonstrated in previous investigations [1,4,7,8] that the morphology of these hybrid systems can be closely controlled by use of suitable coupling agents. Discontinuous, two-phase microcomposites are obtained in the absence of coupling agents, while bicontinuous nanocomposites are obtained by introducing a functional alkoxysilane such as GOTMS in the precursor solution for the formation of silica. The present paper is aimed at a detailed characterization of the hybrid systems taking into consideration several aspects of the problem. It is now clear that most properties of the hybrid materials are affected not only by the overall morphology but also by the molecular structure of the inorganic phase obtained upon curing. The sol–gel chemistry is complex and can certainly be influenced by the presence of the polymeric precursor and its solvents. So far most of the literature reports have focused on the analysis of the organic matrix and on the influence of the silica phase on the imidization mechanism and kinetics [1,7,8]. Much less attention has been paid to the analysis of the inorganic component, partly because it is far less straightforward. We therefore report the results of a quantitative FTIR study on the silica phase of the investigated hybrid samples which was performed by subtraction spectroscopy and curve-fitting analysis. The findings were compared with those obtained on neat silica glasses prepared under the same conditions, in the absence of the polymeric precursor solution.

Regarding the end-properties of the investigated systems, one of the principal issues concerns the sorption of water. This has fundamental implications on the performances of these materials as electrical insulators, on their efficiency in membrane separation processes as well as on their aging behaviour [9–12]. Furthermore, investigations based on a molecular probe like water can enlighten relevant aspects pertaining to the tendency of the polyimide towards the formation of molecular interactions. Thus, we have studied the absorption of water at equilibrium as a function of penetrant activity, comparing the behaviour of the neat polyimide with those of the hybrid systems. The FTIR data also allowed to gather information on the molecular interactions which are established in the investigated systems.

The characterization of the end-properties of the polyimide-based hybrids focused, in the last section of this contribution, on a systematic investigation of the sub-T_g relaxations which

control and determine the excellent tensile properties of these materials [9,11]. The nature of these processes has been under active discussion [13–17] but is, as yet, unclear. In particular, a β transition observed between 50 and 250 °C in PMDA–ODA was initially proposed to arise from interplane slippage in the crystalline phase [13]. Later on, this hypothesis was found to be conflicting with several observations and it was speculated that the β process is related to the mobility of residual amic acid units [18–20]. Subsequent studies pointed to the inconsistency of this proposal [21,22] and to the rise of a further hypothesis, i.e. a rotation–vibration mechanism involving small chain segments around quasi-equilibrium positions [23–25]. In this paper we attempt to interpret the molecular origin of the secondary relaxations in the pure polyimide and to investigate the effect of the inorganic phase on these processes by a detailed dynamic-mechanical analysis coupled with molecular mechanics simulations.

2. Experimental

2.1. Materials

The polyimide precursor used in this study was a polyamic acid, Pyre-ML RK 692 from I.S.T. (Indian Orchard, MA). This has molecular weights $\overline{M}_w = 1.0 \times 10^5$ and $\overline{M}_n = 4.6 \times 10^4$, and is supplied as a 12 wt% solution in a mixture of *N*-methyl-2-pyrrolidone (NMP) and xylene (weight ratio 80/20).

The polyamic acid is obtained by condensation of pyromellitic dianhydride (PMDA) and oxydianiline (ODA). High purity grades of tetraethoxysilane (TEOS) and γ-glycidyloxypropyltrimethoxysilane (GOTMS) were obtained from Aldrich (Milwaukee, WI). Distilled water was used to induce hydrolysis of the alkoxysilane components using a 32 wt% HCl solution as catalyst and ethanol as solvent.

2.2. Preparation of the hybrid films

The alkoxysilane solutions used for the production of microcomposite and nanocomposite films (22.3 wt% silica) were prepared as specified in Ref. [7]. Next, these solutions were added dropwise to the polyamic acid solution under continuous stirring for 10 min at ambient temperature. Castings (20–30 μm thick) were obtained by spreading the above solution onto a glass plate with the aid of a Gardner knife. The cast films were allowed to dry for 1 h at RT and then for 1 h at 80 °C to allow most of the solvent to evaporate. Clear films were obtained for both pure polyimide and the hybrid sample containing GOTMS, while an opaque film was obtained in the absence of GOTMS. Imidization and condensation reaction were carried out in successive isothermal steps of 1 h each, at 100, 150, 200, 250 and 300 °C. Finally, the cured films were peeled off from the glass substrate by immersing in distilled water at 80 °C. Thinner films (2.5–1.0 μm) were obtained by spin-coating a prescribed amount of the precursor solutions onto a glass substrate. The spin-coating was a two-step process performed with a Chemat KW-4A apparatus equipped with an automated fluid dispenser (KW-4AD), from Chemat Technologies Inc., Northridge, CA, USA. The spinning conditions were 12 s at 700 RPM for the first step; 20 s at 1500 RPM for the second step. Curing conditions for the spin-coated films were the same as those for the thick films.

2.3. FTIR spectroscopy

Mid-FTIR spectra were recorded either on powder samples dispersed in dry KBr (for the pure silica samples), or on solution cast films (polyimide and polyimide/silica hybrids) using a System 2000 spectrometer from Perkin–Elmer (Norwalk, CT). This instrument was equipped with a Ge/KBr beamsplitter and a wide-band DTGS detector. The instrumental parameters were as follows: resolution = 4 cm^{-1}, optical path difference (OPD) velocity = 0.2 cm s^{-1}, spectral range = 4000–400 cm^{-1}. Signal averaging was performed for improving the signal-to-noise ratio (64–128 scans). A vacuum tight cell was used to record the FTIR transmission spectra of the polymer films exposed to a controlled humid environment. The cell was connected by service lines to a water reservoir, a vacuum pump and pressure transducers and allows the *in situ* drying of the samples and the *on-line* monitoring of the sorption process. Full details of the experimental set-up are reported in Ref. [26].

2.4. Dynamic-mechanical measurements

Dynamic-mechanical tests were carried out using a Perkin–Elmer *Pyris Diamond DMA* apparatus. The experiments were performed in tensile mode at frequencies of 0.1, 0.5, 1, 2, 5 and 10 Hz at a heating rate of 3 °C min^{-1} and in a temperature range from −150 to +500 °C. Samples 50 mm long, 10 mm wide and 40 μm thick were used. The storage modulus (E'), loss modulus (E'') and loss tangent (tan δ) were recorded.

2.5. Simulation methodology and computational details

Molecular mechanics calculations were made using the MM+ force field, which is an extension of the Allingher's MM2 program [27]. Apart from the standard Potential Energy terms (bond stretching, bending, torsion, van der Waals, H-bonding, electrostatic), the MM+ force field also contains stretch–bend cross-terms (Urey–Bradley). These include 1–3 interactions which are often critical for accurately simulating complex molecules. The potential energy surface of the model compound was explored by a conformational search algorithm. This performs the following steps: (1) starting from an initial structure, modifies it by varying user selected geometry parameters (torsion angles), (2) optimizes the geometry of the modified structure to an energy minimized conformation, and (3) compares the conformation with those found previously and accepts if unique and if it satisfies a criterion. The random-walk Monte Carlo method was adopted for systematic variations in step 2. All computer modelling calculations were performed on a Dell workstation mod; precision 450, having two parallel 2.66 GHz processors (Xeon from Intel, CA, USA). The MM module of the programs' suite

Hyperchem Pro6, from Hypercube Inc (FL, USA) was used throughout.

2.6. Morphology

The films were fractured in liquid nitrogen and the surfaces were examined by scanning electron microscopy (SEM) using a Philips XL20 instrument. Prior to examination the fractured surfaces were coated with a gold–palladium layer by vacuum sputtering.

3. Results and discussion

3.1. Microstructural features of the SiO_2 phase

To investigate the structure of the inorganic phase as developed within the hybrid systems and to compare the results with those obtained for pure silica glasses, a comparative FTIR spectroscopy analysis was performed on the hybrid films and the silica powders.

The transmission spectrum in the 4000–370 cm^{-1} range of the hybrid film containing 22.3 wt% of silica and characterized by a co-continuous nanoscale morphology (nanocomposite) is reported in Fig. 1A. Fig. 1B displays the spectrum of a hybrid system of the same composition, having a two-phase structure with micron-sized silica domains (microcomposite). Both spectra closely resemble that of a fully cured polyimide, with no evidence of residual absorptions characteristic of the amic acid group. This indicates that the inorganic phase has no detrimental effects on the curing of the polyimide component, in agreement with previously published results which showed a catalytic activity of the silica phase towards imidization [7].

The spectra reported in Fig. 1A,B also display two bands characteristic of a condensed silica glass at around 1090 and 460 cm^{-1}, thus confirming the complete development of the inorganic phase in both the hybrid systems. The shape of the above bands, however, albeit partly superimposed onto polyimide peaks, is seen to be significantly different in the two samples, thus indicating a different phase structure of the inorganic component. More information concerning these differences can be obtained by isolating the silica spectrum from that of the composite systems and comparing it with the spectra of pure silica glasses prepared under the same conditions (Fig. 1C,D).

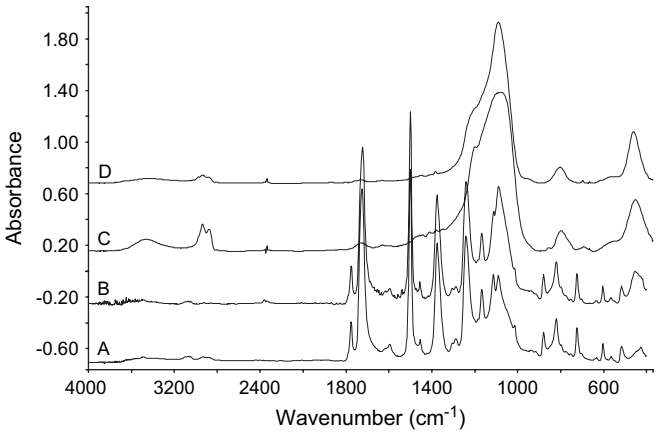

Fig. 1. FTIR transmission spectra in the wavenumber range 4000–370 cm^{-1} of: (A) PI/silica nanocomposite, 22.3% by weight in silica; (B) PI/silica microcomposite, 22.3% by weight in silica; (C) neat silica obtained from a TEOS/GOTMS solution; and (D) neat silica obtained from a TEOS solution.

Before tackling this problem, however, it seems useful to briefly review the interpretation of the silica spectrum according to the most recent studies. For the sample prepared in the absence of the GOTMS coupling agent (see Fig. 1D) there are four distinct absorptions, centred, respectively, at 2930, 1090, 805 and 460 cm^{-1}. The band at higher frequency is related to the C–H stretching modes of residual alkyl groups, while the 1090 cm^{-1} band is a complex profile with multiple contributions having different vibrational origin. In particular, a curve resolving analysis performed according to the method described in Section 2 (see Fig. 2A and Table 1 for a summary of the results) displays four main components at 1219, 1158, 1091 and 1044 cm^{-1}. The doublet at 1091–1044 arises from the asymmetric stretching mode of the Si–O–Si group while the two components at 1219 and 1158 cm^{-1} are likely related to the splitting of the above mode into a well separated transverse-optical/longitudinal-optical (TO–LO) pair [28–30]. A minor contribution to these components of the Si–O–C asymmetric stretching modes cannot be ruled out. The doublet at 1091–1044 cm^{-1} is of particular interest for it carries distinct information on the molecular structure of the inorganic network. In fact, studies conducted on linear and cyclic methylpolysiloxane model compounds, and later substantiated with more complex sol–gel derived silica glasses [31], demonstrated that this absorption appears at lower wavenumbers in going from linear to cyclic structures. It was also noted that, within cyclic molecules, larger rings (i.e. less strained structures) absorb at comparatively lower frequencies. In the light of the above findings, it appears reasonable to attribute the splitting of the ν_a(Si–O–Si) to a discrimination between cyclic (at 1093 cm^{-1}) and linear (at 1044 cm^{-1}) structures.

The 805 cm^{-1} peak is to be attributed to the symmetric Si–O–Si stretching vibration, which is predicted to be infrared inactive but is observed in the spectrum likely because of the lack of coordinative symmetry around the silicon atom. Finally, the peak at 460 cm^{-1} has been assigned to the Si–O–Si bending mode and its position has been shown to be influenced by the equilibrium bond angle [29,31]. Therefore, the width of this peak is a sensitive measure of the distribution of Si–O–Si bond angles which, according to the theoretical models of the silica glass structure, is necessarily broad.

To elucidate the molecular structure of the glass phase obtained in the present preparation conditions, it is also useful to follow the evolution of the infrared spectrum of neat silica with curing temperature. Several studies have appeared in the literature, where data of this type have been reported. Generally, however, the considered temperature range is much wider, reflecting the conditions under which silica glasses are normally produced. Here, instead, we are interested in the structure development at a relatively low process temperature, i.e. up to 300 °C. In Fig. 3A and B are reported,

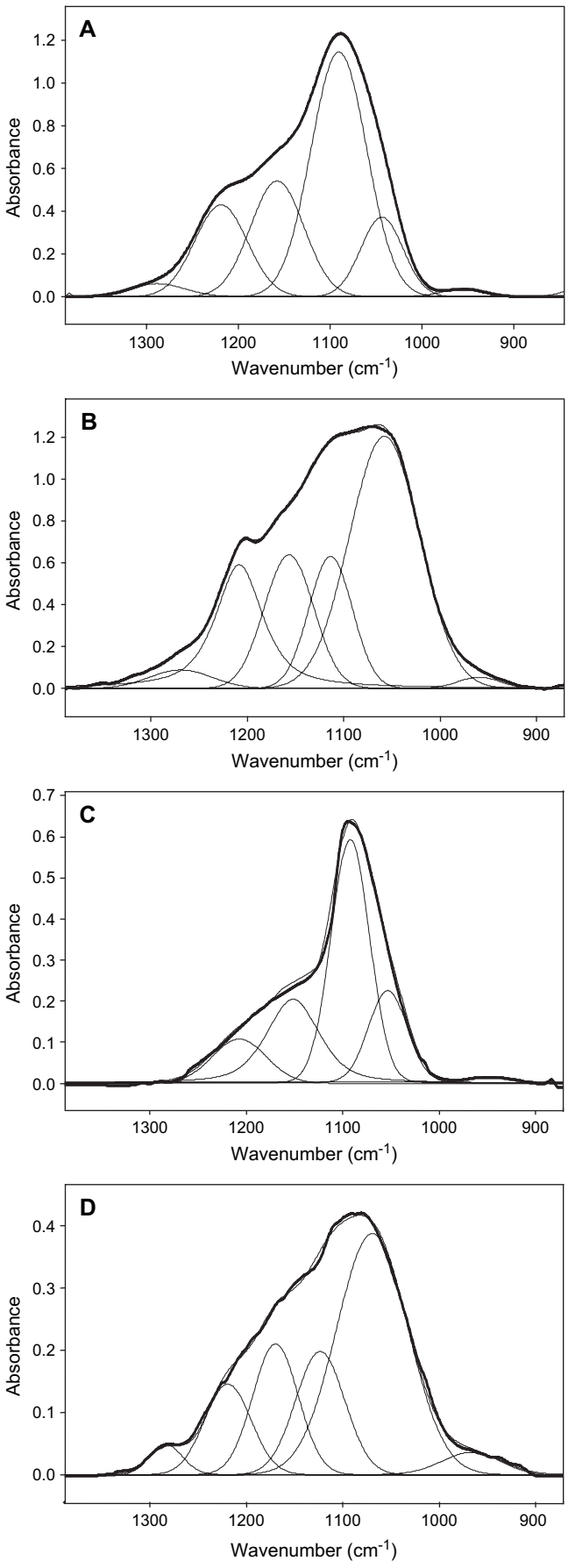

Fig. 2. FTIR transmission spectra and relative curve-fitting analysis in the region 1400–850 cm^{-1} of: (A) neat silica from a TEOS solution; (B) neat silica from a TEOS/GOTMS solution; (C) microcomposite 22.3% by weight in silica; and (D) nanocomposite 22.3% by weight in silica.

respectively, the FTIR spectra in the 4000–2400 cm^{-1} range and in the 1450–370 cm^{-1} range, of the silica treated isothermally for 1 h at increasing temperatures. The more evident features are the reduction of the ν_{OH} band and, in the low frequency side, the gradual evolution of the 1090 cm^{-1} band, accompanied by the almost complete disappearance of the 952 cm^{-1} absorption, due to the stretching vibration of silanol groups (Si–OH). The 800 cm^{-1} band gradually shifts to 806 cm^{-1}, while the bending mode at 460 cm^{-1} narrows in going from 80 to 100 °C and remains essentially constant afterwards. A quantitative analysis of the above spectra is presented in Fig. 4, in terms of band areas, which are proportional to the concentration of the various functional groups.

It is seen that, in the temperature range investigated, the amount of hydroxyl groups displays a decay to almost zero, while the alkyl content remains essentially constant. The above observations indicate that the hydrolysis (step 1 of the sol–gel mechanism) is already complete at 80 °C, leaving a small amount of residual Si–OR groups entrapped in the network. The condensation reaction proceeds essentially by step 3 of the sol–gel mechanism (i.e. water elimination), as indicated by the constant concentration of residual alkyl groups, and is close to completion at 300 °C. This process produces a network in which the cyclic SiO_2 structures (i.e. those highly interconnected) strongly prevail over linear, branched structures. Assuming equal absorptivities for the ν_{as} modes of the SiO_2 unit in the different environments, the final concentration ratio $[SiO_2]_{cyclic}/[SiO_2]_{linear}$ is equal to 4.1 (see Fig. 4).

The presence of GOTMS in the precursor solution of the silica glass strongly influences its evolution with temperature and the final molecular structure obtained thereafter. The spectra collected at the various curing temperatures for the TEOS–GOTMS solution are displayed in Fig. 5A (4000–2400 cm^{-1} range) and in Fig. 5B (1550–370 cm^{-1} range). In the high frequency side the hydroxyl content is found to decrease less gradually than for the neat TEOS solution, and does not vanish at 300 °C; a medium intensity band is observed in the ν_{CH} range, which remains fairly stable with temperature. In the low frequency region the profile centred at about 1100 cm^{-1} evolves quite noticeably with temperature, while the bending mode at 460 cm^{-1} hardly changes. Two peaks at 907 and 852 cm^{-1} are assigned to ring deformation modes of the epoxide group [32,33]. They both decrease gradually up to complete disappearance in a temperature range from 80 to 200 °C, thus confirming the reactivity and complete conversion of the GOTMS epoxy groups. A quantitative analysis based, whenever possible, on the direct evaluation of the band areas, or on curve-fitting analysis for the more complex profiles, is reported in Fig. 6. The overall behaviour of the system is very different from that of the control material (compare Figs. 4 and 6). The hydroxyl group content is found to increase slightly up to 200 °C, followed by a sharp drop

Table 1
Curve-fitting analysis in the 1400–800 cm^{-1} range for the spectra of the two investigated silica glasses, the spectrum of the microcomposite and that of the nanocomposite

TEOS			TEOS/GOTMS			MC			NC		
Position (cm^{-1})	FWHH (cm^{-1})	Rel. area (%)	Position (cm^{-1})	FWHH (cm^{-1})	Rel. area (%)	Position (cm^{-1})	FWHH (cm^{-1})	Rel. area (%)	Position (cm^{-1})	FWHH (cm^{-1})	Rel. area (%)
1288	70	3.0	1271	77	3.9	–	–	–	1284	41	2.9
1219	67	16.2	1207	62	19.9	1210	65	10.5	1219	58	12.1
1158	64	17.6	1154	60	18.8	1152	64	27.0	1165	57	17.0
1091	74	46.9	1110	53	13.5	1092	48	43.5	1120	58	17.4
1044	57	11.7	1058	85	43.5	1050	47	17.8	1065	87	49.6
995	42	0.4	956	34	0.3	950	55	1.2	960	70	1.1

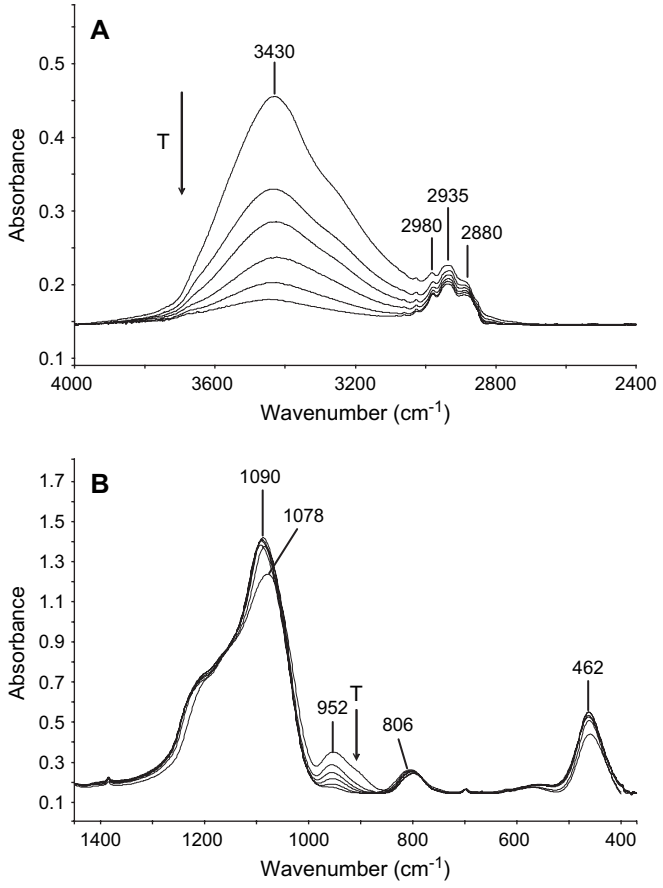

Fig. 3. FTIR transmission spectra of the neat silica from a TEOS solution in a temperature range from 80 to 300 °C; (A) wavenumber range 4000–2400 cm^{-1}; (B) wavenumber range 1450–370 cm^{-1}.

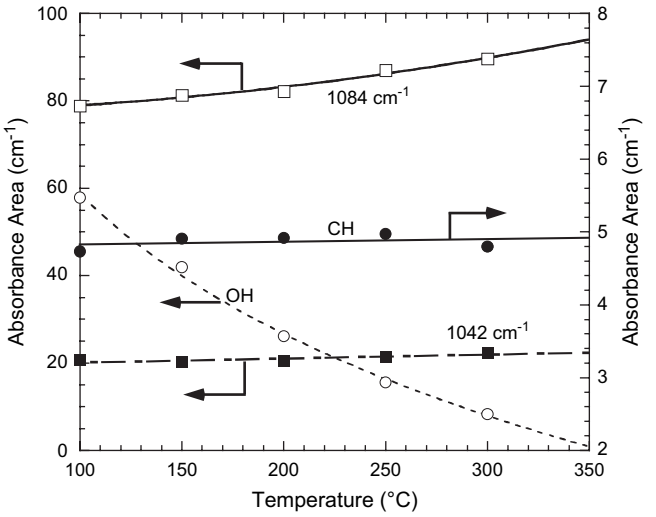

Fig. 4. Absorbance area of peaks corresponding to different functional groups as a function of the curing temperature for a neat silica prepared from a TEOS solution.

at higher temperatures. However, at 300 °C the residual OH group content is about 2.5 higher than for the pure TEOS solution. The slight initial increase can be accounted for by incomplete hydrolysis at 80 °C, which continues up to 200 °C, while it is clear that condensation reactions take place at a substantial rate only above 200 °C. The reacting GOTMS units introduce alkyl chains permanently bound within the silica network, as seen by the occurrence of the intense ν_{CH} band. These groups tend to introduce defects within the inorganic network so as to distort its regularity. As a consequence, the less interconnected and less regular SiO_2 structures tend to be favoured. In fact, in this case, the analysis of the $\nu_{as}(SiO_2)$ region shows that the peak at lower frequency (1057 cm^{-1}), due to the linear, branched structures strongly prevails over the component originating from the cyclic structures, which occurs at 1113 cm^{-1}, and the ratio of $[SiO_2]_{cyclic}/[SiO_2]_{linear}$ goes from 4.1 to 0.31.

The reduction of structural regularity and interconnectivity brought about by the presence of the GOTMS component is also reflected in a broader distribution of Si–O–Si angles, as demonstrated by analysis of the SiO_2 bending peak, whose full width at half height (FWHH), as already mentioned, is directly proportional to the above distribution. In the pure TEOS system the peak occurs at 463 cm^{-1} and has a FWHH of 52 cm^{-1}, while in the TEOS/GOTMS system its maximum occurs at 456 cm^{-1} and its FWHH increases to 71 cm^{-1} (see Fig. 7).

When considering the hybrid systems, an analysis of the inorganic phase evolution as a function of temperature is unfeasible because of the complexity of the spectrum and the simultaneous occurrence of solvent desorption and polyimide curing [7]. Therefore, only the fully cured samples have been considered. In order to isolate the spectrum of the silica phase, difference spectroscopy was employed, subtracting out the spectrum of a fully cured polyimide film from that of the hybrid system. The difference spectrum relative to the

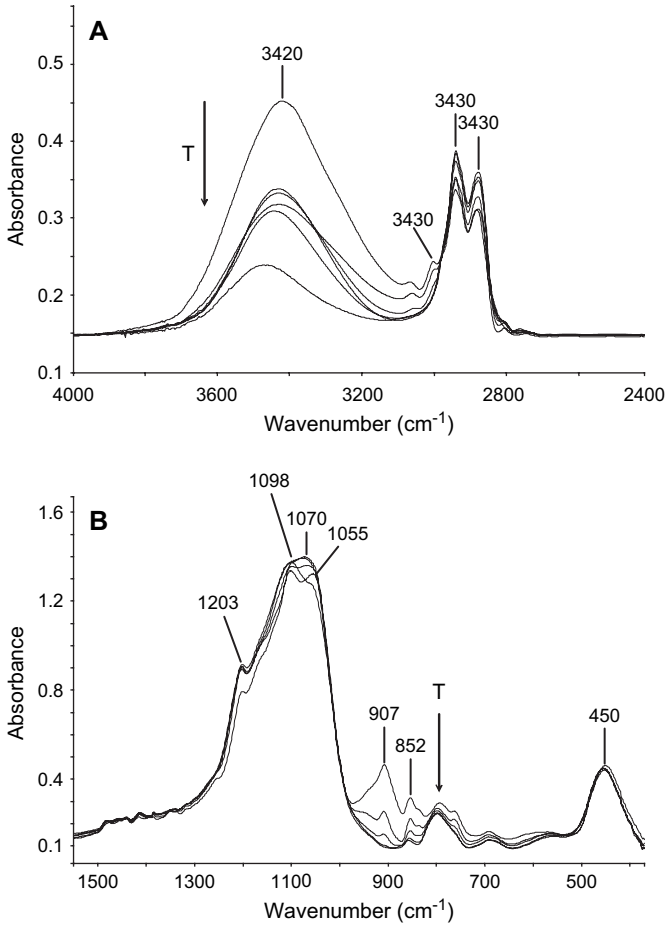

Fig. 5. FTIR transmission spectra of the neat silica from a TEOS/GOTMS solution in a temperature range from 80 to 300 °C; (A) wavenumber range 4000–2400 cm^{-1}; (B) wavenumber range 1550–370 cm^{-1}.

microcomposite in the range 1400–850 cm^{-1} is reported in Fig. 2C along with the results of its curve-fitting analysis. The overall shape of the profile is remarkably similar to the one obtained in the case of the pure TEOS solution cured under the same conditions (compare Fig. 2A and C), apart from the component at 1210 cm^{-1} which shows a reduced intensity in comparison to the reference spectrum of Fig. 2A. In this respect, it is to be noted that in the same region the polyimide shows a very intense absorption which may induce a certain degree of distortion in the difference spectrum. However, we are primarily interested in the doublet at 1082–1035 cm^{-1}, which is not perturbed by interfering absorptions and is reliably isolated by subtraction analysis. It is found that the strongly prevailing components is the one at 1082 cm^{-1}, associated with the ν_a(Si–O–Si) mode in highly interconnected, cyclic structures. The component due to the same vibrational mode in linear structures occurs at 1035 cm^{-1} and displays a much lower intensity. The concentration ratio $[SiO_2]_{cyclic}/[SiO_2]_{linear}$, evaluated from the absorbance ratio of the above peaks, is equal to 4.9, in good agreement with the value of 4.1 obtained for the case of the pure TEOS solution. The O–Si–O bending mode occurs at 456 cm^{-1} and displays a FWHH of 49 cm^{-1}, thus revealing a distribution of interbond angles similar to that of the

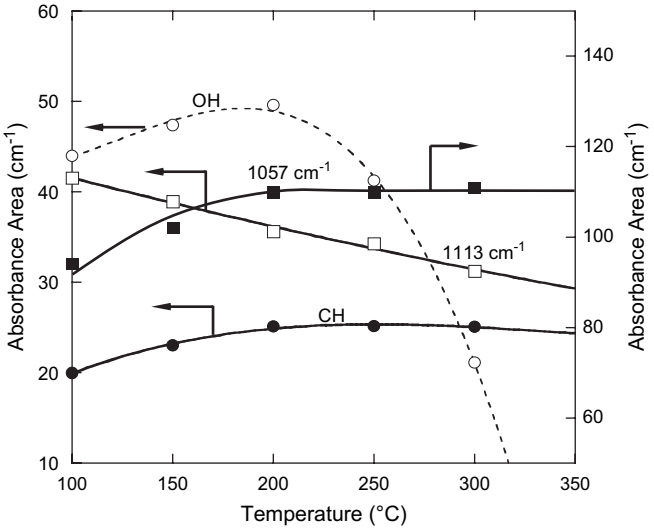

Fig. 6. Absorbance area of peaks corresponding to different functional groups as a function of the curing temperature for a neat silica prepared from a TEOS/GOTMS solution.

neat silica phase. It may be concluded that the molecular structure of the inorganic phase realized in the microcomposite (and, presumably, also its evolution with curing temperature) closely resembles that observed in the absence of the polymeric component. This, in turn, points to an early development of a two-phase structure with (poly)amic-acid forming the continuous phase and the TEOS partially hydrolysed solution forming a fine and homogeneous droplet dispersion within the matrix. In these conditions the subsequent hydrolysis and condensation of the silica phase can proceed with no interference from the surrounding organic phase. The early phase separation of the system is likely induced by the fast evaporation rate of the polyamic acid solvent (NMP), which has been shown to be considerably enhanced by the presence of the TEOS component [7].

The difference spectrum relative to the nanocomposite is shown in Fig. 2D. As in the case of the microcomposite, the spectral profile is similar to that observed for the silica glass prepared from the TEOS/GOTMS solution (compare Fig. 2B and D). The prevailing component is located at 1065 cm^{-1}

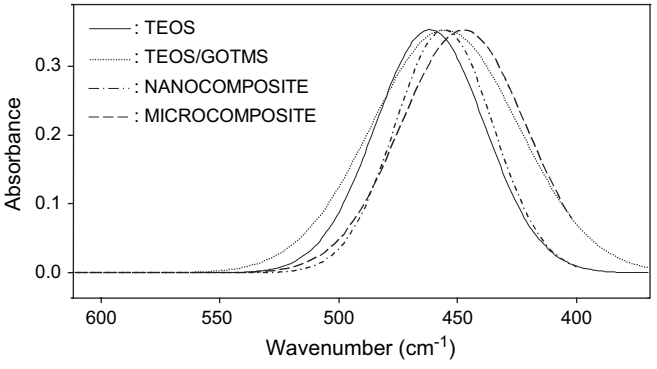

Fig. 7. Absorbance peak relative to the O–Si–O bending mode for the neat silica from a TEOS solution; the neat silica from a GOTMS/TEOS solution; the nanocomposite containing 22.3 wt% of silica and the microcomposite containing 22.3 wt% of silica.

and corresponds to the loosely interconnected, predominantly linear SiO_2 chains. The absorbance ratio between the components at 1065 and 1120 cm^{-1}, which corresponds to the concentration ratio $[SiO_2]_{cyclic}/[SiO_2]_{linear}$ is equal to 0.35, in good agreement with the value of 0.31 obtained for the corresponding silica glass. A residual absorption is clearly detected at 957 cm^{-1}, indicating incomplete conversion of Si–OH groups. The O–Si–O bending mode is found at 445 cm^{-1} and displays a FWHH of 61 cm^{-1}, lower than that of the parent silica, but considerably higher that those of the microcomposite and of the silica glass prepared without GOTMS. Again, the experimental observations point to a molecular structure of the silica phase analogous to that obtained in the absence of the polymer precursor. Concerning the important point of the coupling agent reactivity, we have no direct spectroscopic evidence because of the low intensity of the oxirane peak and the severe overlapping of interfering absorptions. However, the conclusion that in the nanocomposite the inorganic phase has the same features as those of the pure silica prepared under the same conditions and is significantly different from the structure realized in the absence of GOTMS is an indication that the GOTMS epoxy groups react with the Si–OH groups, rather than with other functionalities present in the system, such as the carboxylic and/or amide moieties of the polyamic acid. Therefore, the strong influence of GOTMS on the final morphology of the hybrid system is to be related to the phase separation mechanism (spinodal decomposition), and, in particular, to a decrease in the rate of particle-growth [4].

3.2. H_2O sorption and molecular interactions

To investigate the water sorption behaviour, the pure polyimide, the microcomposite and the nanocomposite samples were subjected to sorption processes at different water vapour activities until they reached equilibrium, and the isothermal curves so obtained were compared. The measurements were carried out in a specially designed diffusion cell (see Section 2) located in the sample compartment of the FTIR spectrometer to allow the *in situ* monitoring of the sorption process. It is important to note that, when analyzing the evolution of the polyimide spectrum as a function of water uptake and, in particular, the evolution of the intense ν_{oop} carbonyl peak, it is mandatory to work with film thickness between 1.0 and 2.5 μm to avoid signal saturation. These films were prepared *ad hoc* by a spin-coating process and have been demonstrated to reach water saturation in very short times (few seconds). This implies the necessity of performing the drying process *in situ* insofar as it is not possible to manipulate a dry sample in the atmosphere.

In Fig. 8 the FTIR transmission spectrum of the dry polyimide film is compared with the spectrum of the same sample equilibrated at $a = 0.8$ in the wavenumber range 1900–500 cm^{-1}. The main feature emerging in the water saturated sample is a broad absorption at around 1620 cm^{-1}, which is due to the in-plane bending (δ) of absorbed water. This band can be suitably isolated by spectral subtraction, i.e. by subtracting the spectrum of the dry sample from that of the water containing sample; the results of such an analysis, for the various investigated activities, are reported in the inset of Fig. 8.

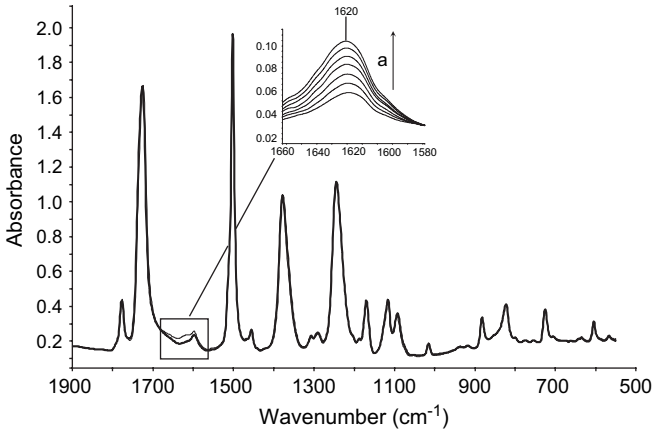

Fig. 8. Transmission FTIR spectra in the 1900–500 cm^{-1} interval for the pure PMDA–ODA polyimide in the dry state (thick line) and after equilibration at $a_w = 0.8$ (thin line). In the inset is displayed the δ band of water for the various investigated activities, as obtained by subtraction spectroscopy.

From the absorbance area of the δ band it is possible to evaluate the concentration of absorbed water by the use of a calibration curve constructed by combining gravimetric and spectroscopic sorption data [34]. The results of the quantitative analysis are reported in Fig. 9. It is seen that the pure polyimide absorbs a relatively low amount of H_2O (up to 2.5 wt% at $a = 0.8$) in agreement with previously reported literature data [35–38]. Water uptake increases substantially in the case of the nanocomposite (up to 4.1 wt% at $a = 0.8$) as a consequence of the hydrophilic nature of the silica phase, which is able to form molecular interactions of the H-bonding type with water through the Si–OH groups. Quite surprisingly,

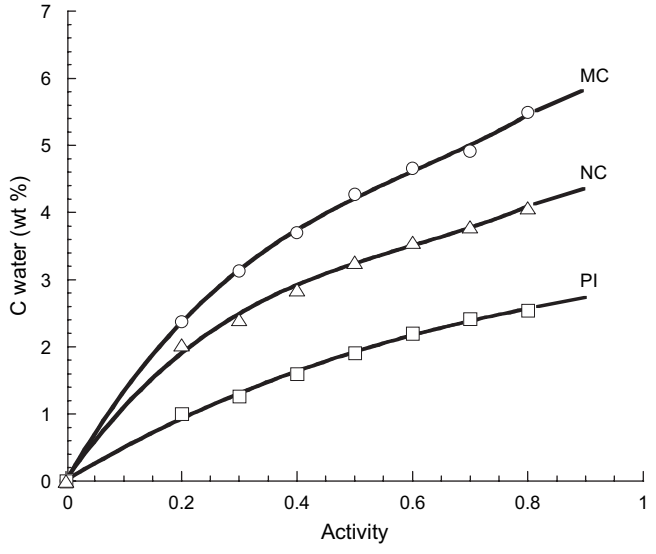

Fig. 9. Water sorption isotherms for pure polyimide, the nanocomposite (NC) and the microcomposite (MC). Both hybrid samples contain 22.3 wt% of silica.

the microcomposite exhibits a water uptake well above that of the nanocomposite, although in the previous paragraph it has been shown that the microstructure of the silica phase is more compact and the number of residual Si–OH groups is lower in the microcomposite than in the nanocomposite. A possible explanation of this effect is the occurrence of interstitial space between the polymeric phase and the completely debonded inorganic phase, which could provide an empty volume in which diffusing water molecules could be accommodated (see micrograph of Fig. 17A). Work is in progress to substantiate this hypothesis and to gain a deeper understanding of this interesting effect.

A closer look at the differences between the spectra of *dry* and *wet* samples evidences a consistent shift of both the carbonyl stretching modes (i.e. ν_{ip} at 1777 cm^{-1} and ν_{oop} at 1726 cm^{-1}) towards lower wavenumbers. This is demonstrated in Fig. 10, which also shows that the shift magnitude is directly proportional to the amount of water present in the sample. The effect is fully reversible, i.e. both peaks revert to their original positions upon removal of the absorbed water. Evidently, the imide carbonyls are involved in H-bonding type interactions as proton acceptors with water molecules acting as donors. The molecular interaction causes a lowering of the carbonyl force constant (a decrease of the bond order) with a consequent reduction of the resonance frequency.

The same effect is found for the nanocomposite and the microcomposite samples, and the shift values at all investigated activities are comparable in magnitude for the three systems. This implies that the extent and the mechanism of the imide–H_2O interaction does not change in the presence of the inorganic phase and confirms that the excess of absorbed water in the hybrid systems with respect to neat polyimide is actually due to absorption in the inorganic phase.

The above results demonstrate that the carbonyl peaks are a very sensitive probe for the occurrence of molecular interactions. It is therefore expected that a comparison between the peaks' position as determined in the pure polyimide and in the two hybrid systems could highlight possible molecular interactions between the polymeric matrix and the inorganic phase. It is explicitly noted that, for this comparison to be meaningful, it is mandatory that the samples are fully dried insofar as the presence of water causes significant peak shifts. Inspection of Fig. 11 reveals that the ν_{oop} frequencies are exactly coincident in the polyimide and in the microcomposite, thus confirming the complete absence of interactions among the two phases in this system. Conversely, in the case of the nanocomposite, a small shift towards higher frequencies (0.45 cm^{-1} for the ν_{ip} peak and of 0.70 cm^{-1} for the ν_{oop}) is detected. From this observation two conclusions can be drawn:

(i) A modest yet detectable perturbation of the force constant of the imide carbonyls and/or of the molecular geometry of the *N*-phenyl substituted imide units takes place in the nanocomposite, which is indicative of molecular scale proximity between the phases.

(ii) Although the present study has demonstrated that the imide carbonyls are capable of forming H-bonding interactions as proton acceptors, and therefore could, in principle, interact with the Si–OH groups of the inorganic phase, the spectroscopic results conclusively demonstrate that this type of interaction does not occur. In fact, such a mechanism would have produced a shift of the carbonyl bands towards lower wavenumbers, i.e. in the direction opposite to that actually observed. This conclusion seems of particular relevance insofar as several authors have postulated the occurrence of the above H-bonding interaction in PI/SiO_2 hybrid systems [39,40].

At the moment the molecular mechanism giving rise to the observed carbonyl shift is unclear. Several hypotheses can be put forward, among which the possibility that the presence of a molecularly interconnected silica phase may reduce the tendency of the polyimide chains towards self-association through intermolecular chain-transfer interactions (CTI) [41]. Thus, it is possible that imide units not involved in CTI experience an increased localization of the electronic density on the C=O bonds with a consequent increase of the relative force constant and a corresponding high frequency shift. An

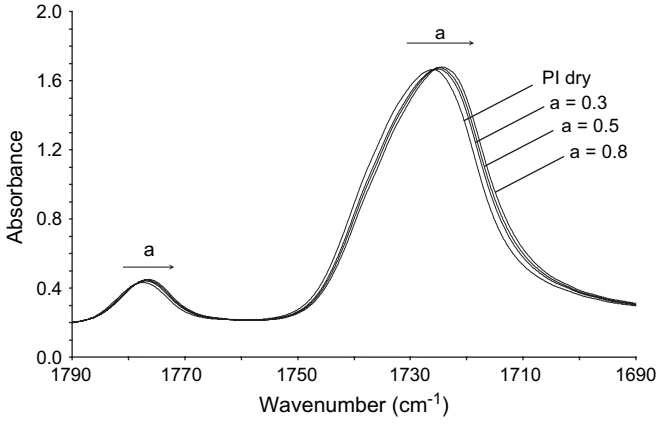

Fig. 10. The carbonyl region of PMDA–ODA polyimide in the dry state and equilibrated at different water vapour activities.

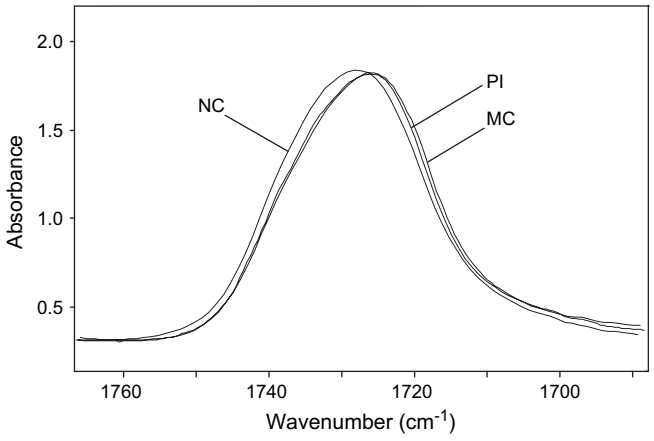

Fig. 11. The ν_{oop} carbonyl peaks of the polyimide, the nanocomposite and the microcomposite in the dry state.

influence of the silica phase on the conformational equilibrium of the *N*-phenyl substituted imide units, along the N–Ph bond is also possible. In any case, in the light of the relatively modest effect, it seems likely that the silica phase plays an indirect role in stabilizing otherwise energetically unfavored molecular structures of the polyimide chains, rather than forming a well defined interaction complex.

3.3. Dynamic-mechanical analysis and molecular mechanics simulations

The storage modulus (E') and the loss factor tan δ at 1 Hz for the pure polyimide, the microcomposite and the nanocomposite samples are shown, respectively, in Figs. 12 and 13.

The presence of silica increases the elastic modulus both in the glassy region and at temperatures above the glass transition. The upturn in the E' curves above the glass transition is likely to result from intermolecular crosslinking reactions. The tan δ plots reveal the occurrence of three relaxation processes: the low and the medium temperature relaxations are defined, respectively, as the γ and β transitions (Fig. 13a). The high temperature peak is an α-relaxation process and corresponds to the glass transition (Fig. 13b). The β transition displays an asymmetrical shape and occurs over a very wide temperature range. It has been generally associated with local bond rotations along the polyimide backbone, although its exact description is still uncertain [13,42–44]. The nature of this relaxation process will be discussed in detail later, in connection with the molecular simulation studies.

The lowest-temperature γ transition has been observed previously in a limited number of studies and only in the presence of absorbed moisture. From the data of Fig. 13, two observations can be made with respect to the incorporation of the silica phase within the polyimide matrix. The first is that the γ, β and α peaks are displaced towards higher temperatures (see Table 2). The increase in T_β and T_α is about 10 °C for the microcomposite and, respectively, of 24 °C and 34 °C for the nanocomposite. The T_γ increase is considerably lower. The second observation is that the height of these transitions decreases. The effect is larger for the β and α processes and is much more pronounced for the nanocomposite sample.

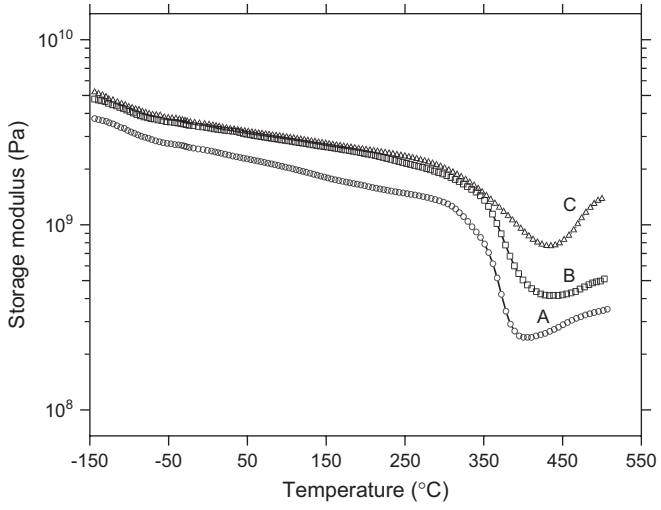

Fig. 12. Storage modulus (E') as a function of temperature for (A) pure polyimide; (B) the microcomposite containing 22.3 wt% of silica; and (C) the nanocomposite containing 22.3 wt% of silica.

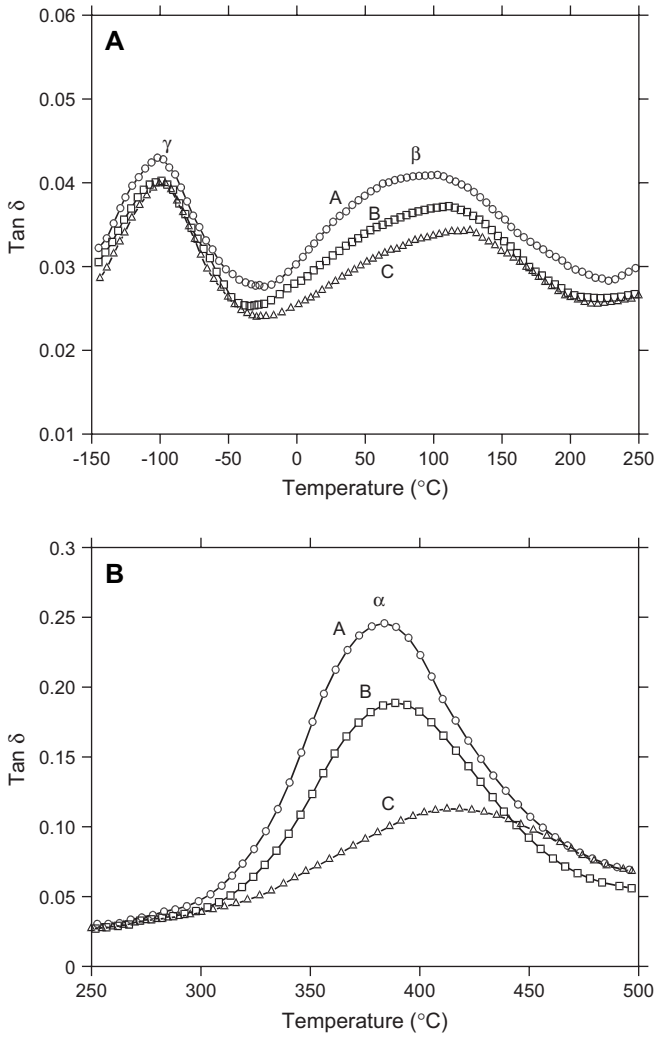

Fig. 13. Tan δ spectra as a function of temperature for (A) pure polyimide; (B) the microcomposite containing 22.3 wt% of silica; and (C) the nanocomposite containing 22.3 wt% of silica. A: Temperature range: −150–250 °C; B: temperature range: 250–500 °C.

Further details on the effect of the silica phase were gathered by a multi-frequency analysis. Fig. 14 shows the tan δ vs temperature curves collected at five different frequencies on the nanocomposite sample. It is found that, by increasing the frequency, the peak maxima shift at higher temperatures while the intensities decrease. A similar behaviour has been observed for the microcomposite and the control resin. The

Table 2
The γ-, β- and α-relaxation temperatures at 1 Hz and the activation energies for polyimide, microcomposite and nanocomposite

Sample	T_γ (°C)	γ E_a (kcal/mol)	T_β (°C)	β E_a (kcal/mol)	T_α (°C)	α E_a (kcal/mol)
Polyimide	−103	10.3	102.2	22.7	384	240.1
Microcomposite	−98	10.0	111.2	24.9	394	252.0
Nanocomposite	−94	11.5	126.2	36.9	418	284.3

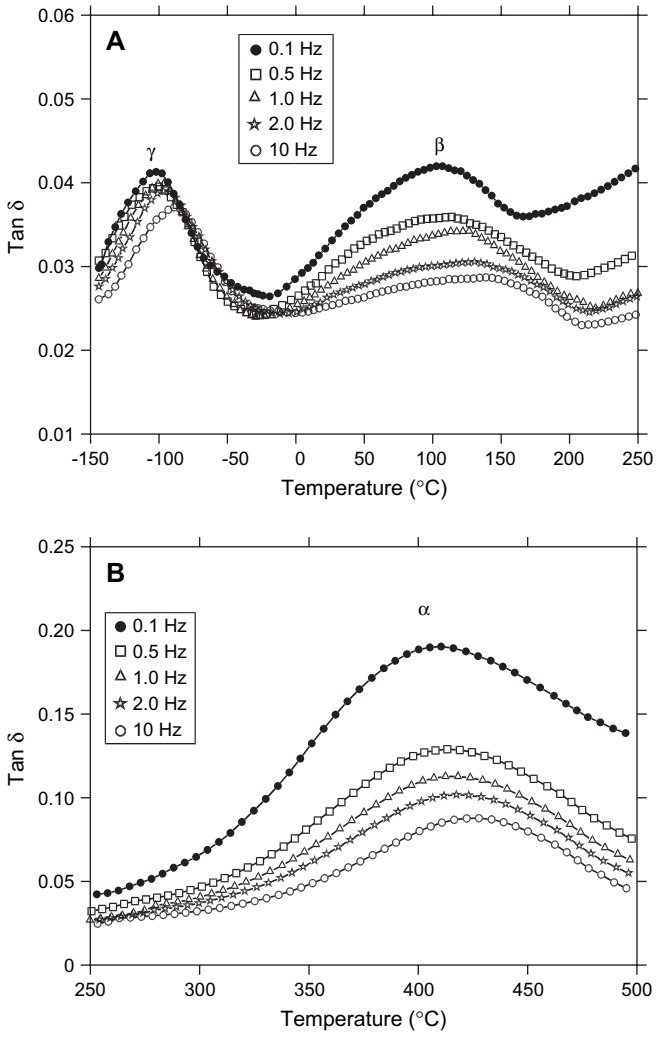

Fig. 14. Tan δ spectra as a function of temperature for the nanocomposite sample containing 22.3 wt% of silica, at different frequencies. A: Temperature range: −150–250 °C; B: temperature range: 250–500 °C.

above frequency dependence has been examined using the Arrhenius equation:

$$f = A\, e^{\frac{-E_a}{RT}} \tag{1}$$

where f is the frequency, A is the pre-exponential factor, R is the gas constant, T is the absolute peak temperature and E_a is the activation energy.

The above equation is generally suitable for non-cooperative processes (i.e. sub-T_g relaxations). For long-range motions (α transitions) the method remains satisfactory if applied within a relatively narrow range of frequencies (two to three orders of magnitude), although the E_a so obtained represents a limiting or apparent value. The Arrhenius equation has been employed for the γ, β and α transitions of the hybrid materials and the parent polyimide, as shown in Fig. 15 where the logarithm of frequency is plotted vs $1/T$, relative to the β relaxation process. Analogous diagrams were obtained for the γ and α transitions. The activation energies determined from the slope of the Arrhenius plots are summarized in Table 2. For the microcomposite the values differ slightly from those

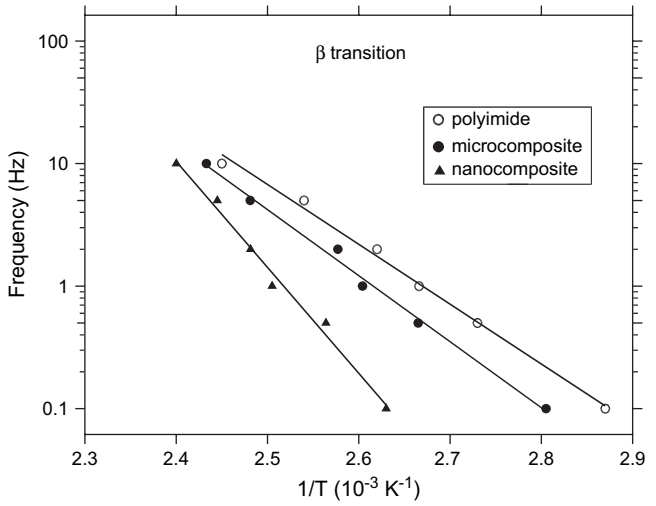

Fig. 15. Arrhenius plot relative to the β transition for the polyimide, the nanocomposite and the microcomposite.

of the parent polyimide, while a significant enhancement is found for the nanocomposite, especially for the activation energies related to β and α transitions.

The role of the silica phase on the β relaxation as well as the type of molecular motions involved in this process can be further elucidated by using the theory proposed by Starkweather [45,46]. This approach allows us to separate the overall activation energy into an activation enthalpy term (ΔH^+) and an activation entropy term (ΔS^+) through the Eyring theory of the absolute reaction rate [44]:

$$f = \frac{kT}{2\pi h}\exp\left(\left(-\frac{\Delta H^+}{RT}\right)\exp\left(\frac{\Delta S^+}{R}\right)\right) \tag{2}$$

where k and h are the Boltzman and Planck constants, respectively, R is the gas constant and f is the frequency.

The relation between the activation energy and the activation enthalpy is given by

$$E_a = \Delta H^+ + RT \tag{3}$$

In Eq. (3) the Arrhenius activation energy is

$$E_a = R\frac{d(\ln f)}{d(1/T)} \tag{4}$$

and the Eyring activation enthalpy is

$$\Delta H^+ = -R\frac{d(\ln f)}{d(1/T)} \tag{5}$$

Combining Eqs. (2) and (3), we obtain

$$E_a = RT\left[1 + \ln(k/2\pi h) + \ln(T/f) + T\Delta S^+\right] \tag{6}$$

Starkweather found that for many relaxation processes, particularly those involving the motion of small segments, the activation entropy is close to zero. Under this assumption the activation energy follows a simple, linear dependence with temperature:

$$E_a = RT'[1 + \ln(k/2\pi h) + \ln T'] \tag{7}$$

where T' is the temperature of the maximum of the β peak observed at 1 Hz.

The difference between the experimental activation energy and this theoretical value is equal to $T\Delta S^{+}$. Thus Eq. (7) defines an effective lower limit for the activation energies of viscoelastic processes.

For the pure polyimide Eq. (7) gives an activation energy of 21.9 kcal/mol. This value is close to that obtained experimentally (see Table 2), indicating that the motion involved in the β relaxation process is basically non-cooperative, in agreement with most of the literature results. For the micro- and nanocomposite samples the values derived from the Starkweather analysis are, respectively, 22.05 and 23.05 kcal/mol, which differ significantly from those reported in Table 2. This implies that for the hybrid materials the ΔS^{+} value is significantly higher than zero and the relaxations involved display a greater degree of cooperativity in comparison to the pure polyimide.

To account for the results of the preceding analysis, and in view of the still controversial description of secondary relaxations mechanisms in polyimide systems, we performed a computer modelling study aimed at a deeper understanding of their molecular origin.

The first step in the calculation was to establish a suitable molecular model to simulate the behaviour of the polymer chain. Being interested in localized, non-cooperative motions, we restricted our attention to a fragment comprising a single pyromellitic dianhydride unit reacted with two 4-phenoxy aniline molecules (Scheme 1).

This model compound allows us to investigate the main conformational degrees of freedom. From inspection of Scheme 1 and according to previous literature reports [17], two possibilities of a non-cooperative motion exist: (i) rotation of the whole plane of the pyromellitic unit through the concurrent rotation around the two N–C bonds, and (ii) rotation of the plane of the *p*-disubstituted phenylene unit by the concurrent rotation around the N–C and C–O bonds. The next step of the calculation was to establish an initial geometry, that is, a minimum energy conformation (stationary state) to be used as reference state for evaluating the energy requirements for a localized motion to occur. We recall that for the molecular mechanics approach only energy differences between two conformations are significant, while absolute energy values are meaningless. As it can be easily recognized, the potential energy surface of the model compound I is quite complex. To explore it in some detail, a conformational search (CFS) was performed (see Section 2 for details), by systematically varying the torsion angles τ_1, τ_2, τ_3, τ_4, τ_5 and τ_6 that are indicated in Scheme 1. The minimum energy conformation is that shown in Scheme 1, and the contributing energy terms are collectively reported in Table 3. It is to be noted that the potential energy surface as evaluated from CFS, is very shallow and several, almost isoenergetic conformations (within few cal/mol) are identified. They essentially differ for the relative positions of the two terminal phenyl rings, i.e. for the τ_1–τ_2 and the τ_5–τ_6 torsion angles. However, the conformational analysis performed on higher energy conformers demonstrated that the main findings are essentially unaffected if one considers these latter as the reference state. The strategy adopted to simulate a localized, non-cooperative motion was a modified version of the rigid rotor approximation (RDA). Unlike conventional calculations of the rotational energy barrier which rely on varying a single torsional angle along a bond, while holding rigid the two ends of the molecule, in the present case the two terminal bonds connecting the rotating

Table 3
Geometry and energy parameters corresponding to the minimum energy conformation and to the energy maxima of Fig. 16A,B

	Minimum	Maximum 1[a]	Maximum 2[b]
τ_1	87.54	87.54	87.54
τ_2	87.04	87.04	147.04
τ_3	59.92	176.92	176.27
τ_4	−59.01	−179.01	−59.01
τ_5	92.22	92.22	92.22
τ_6	−88.52	−88.52	−88.52
E_{tot}	91.96	101.97	98.49
E_{str}[c]	1.19	1.18	1.18
E_{bnd}[d]	69.27	69.27	69.27
E_{tor}[e]	−17.97	−20.74	−19.37
E_{vdW}[f]	11.21	23.98	19.13
$E_{str-bnd}$[g]	−0.43	−0.42	−0.43
E_{elect}[h]	28.69	28.69	28.69

[a] Geometry corresponding to the energy maximum of Fig. 16A.
[b] Geometry corresponding to the energy maximum of Fig. 16B.
[c] $E_{str}(\text{kcal/mol}) = \sum_{\text{bonds}} \frac{1}{2} K_r (r - r_0)[1 - \text{CS}(r - r_0)]$.
[d] $E_{bnd}(\text{kcal/mol}) = \sum_{\text{angles}} \frac{1}{2} K_\vartheta (\vartheta - \vartheta_0)^2 [1 + \text{SF}(\vartheta - \vartheta_0)^4]$.
[e] $E_{tor}(\text{kcal/mol}) = \sum_{\text{dihedral}} \frac{V_n}{2} [1 + \cos(n\phi - \phi_0)]$.
[f] $E_{vdW}(\text{kcal/mol}) = \sum_{ij \in \text{vdW}} \varepsilon_{ij} (k_1 e^{-k_2 \rho_{ij}} - k_3 \rho_{ij}^{-6})$.
[g] $E_{str-bnd}(\text{kcal/mol}) = \sum_{\text{angles}} K_{sb} (\vartheta - \vartheta_0)_{ikj} [(r - r_0)_{ik} + (r - r_0)_{jk}]$.
[h] $E_{elect}(\text{kcal/mol}) = \sum_{ij \in \text{polar bonds}} \mu_i \mu_j \left[\frac{\cos\chi - 3\cos\alpha_i \cos\alpha_j}{R_{ij}^3}\right]$.

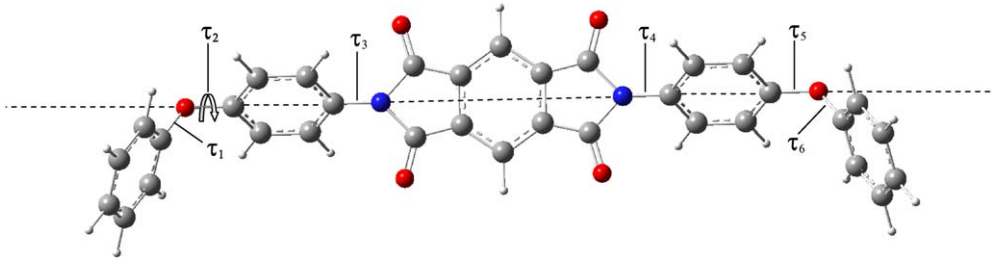

Scheme 2.

unit with the two fixed end-units are simultaneously increased stepwise, while keeping fixed the rest of the structure. For example, to analyze the central pyromellitic unit in Scheme 2, the two τ_3 and τ_4 torsions are stepped, while for the phenylene unit next to it, the torsion angles τ_4 and τ_5 are varied. For each value of the two angles a single-point calculation is performed without further minimization, and the energy values so obtained are plotted as a function of the dihedral angle Φ formed by the plane of the rotating unit at the various τ values and the same plane in the initial reference state (Scheme 2). The Φ angle is changed from 0° to 180° in view of the symmetry of the energy diagram in the interval from 180° to 360°.

In Fig. 16A,B are reported, respectively, the potential energy profiles for the rotation of the pyromellitic unit and the *p*-substituted phenylene unit. The plot relative to the pyromellitic unit displays a pronounced maximum at $\Phi = 120°$, corresponding to an activation energy of 10.0 kcal/mol. The maximum energy conformation corresponds to coplanarity of the pyromellitic unit with the two lateral phenylene rings and arises from a van der Waals interaction term increasing from 11.21 to 23.98 kcal/mol. The profile relative to the phenylene group shows a main peak with a less pronounced shoulder at higher angles; in this case the energy barrier is 6.5 kcal/mol. In comparing the computational results with the experimental findings, we note that, although the experimental activation energy for the γ transition (10.3 kcal/mol, see Table 2) is coincident with the energy barrier for the pyromellitic unit rotation, we disregard the possibility of the γ peak to be related to such a motion. This is in view of the many evidences presented in the literature, and confirmed by our experiments that the γ peak is strongly influenced by the presence of absorbed water in the sample, and thus related to molecular motions partly or totally involving H_2O molecules. Conversely, the experimental activation energy of the β transition (22.7 kcal/mol) is compatible with the mechanism involving the pyromellitic plane rotation. The fact that the experimental E_a is higher than the calculated one is not surprising for the latter is to be regarded as a lower limiting value. In fact the simulation is carried out on an isolated molecular fragment, thus ignoring intermolecular interactions which may play a role in the actual relaxation process. In particular, in the case of polyimides, it is well known that charge-transfer interactions are present. In summary, in the light of the experimental findings and of the simulation results, it is concluded that the β transition in the PMDA–ODA polyimide is to be related to the non-cooperative rotation of the phenylene unit, which occurs easily and at lower temperatures, and the rotation of the pyromellitic unit taking place in the higher temperature side of the transition. The occurrence of these two different motions accounts for the broad and asymmetric profile of the β band. For the microcomposite sample the overall activation energy increases only slightly, while a more pronounced effect is found for the nanocomposite. However, if we consider the results of the Starkweather analysis, we see that the E_a increase is to be attributed to a significant ΔS^+ contribution, while the ΔH^+ term remains very close to that of the pure polyimide. Thus, the presence of a molecularly interconnected silica phase has a twofold effect: (i) it tends to increase the cooperativity character of the units still available to undergo a β relaxation process and (ii) it reduces considerably the number of chain segments involved in the β transition.

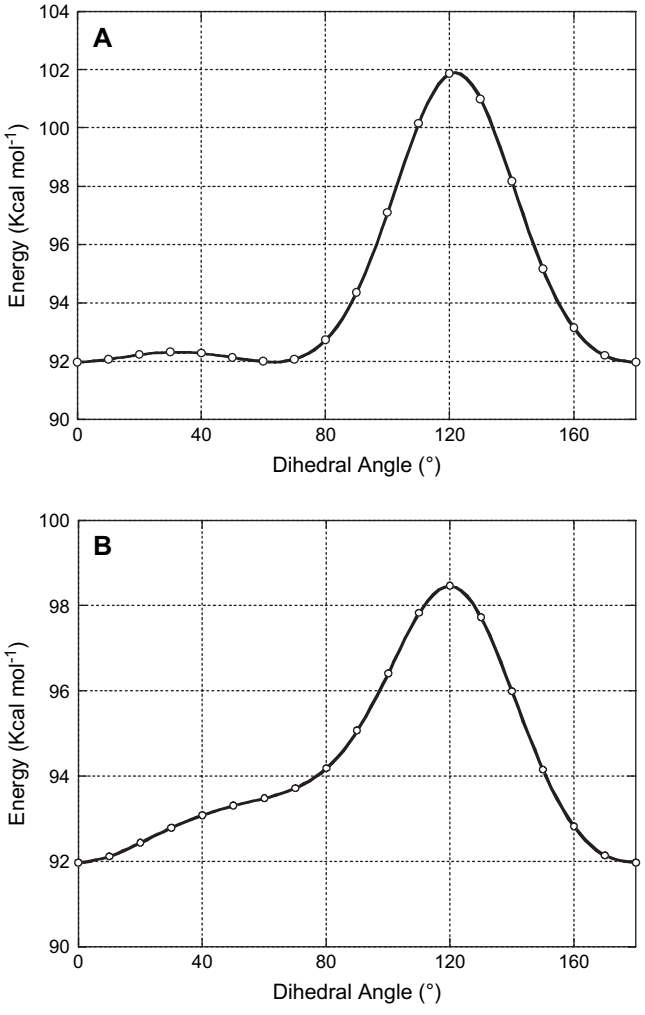

Fig. 16. Energy vs dihedral angle diagram relative to the pyromellitic group rotation (A) and to the phenylene unit rotation (B).

Both the dynamic-mechanical data and the computational results point to an increased constrain on the mobility of short chain segments due to the occurrence of interactions between the silica phase and the polyimide matrix. These interactions are much larger for the nanocomposite than for the microcomposite and can be interpreted in the light of the morphology transition induced by the GOTMS coupling agent. The effect of the GOTMS addition is clearly seen in the micrographs of Fig. 17: a dispersed-particle phase structure is obtained in the absence of GOTMS (Fig. 17A), while a fine interconnected or co-continuous phase morphology is achieved with the use of GOTMS (Fig. 17B). For the compatibilised system (nanocomposite) the size of the interconnected silica domains ranges from 40 to 100 nm, while for the microcomposite system the average diameter of the silica particles varies from 0.8 to 1.2 μm. These two types of morphologies differ considerably to the extent of phase connectivity, with the co-continuous

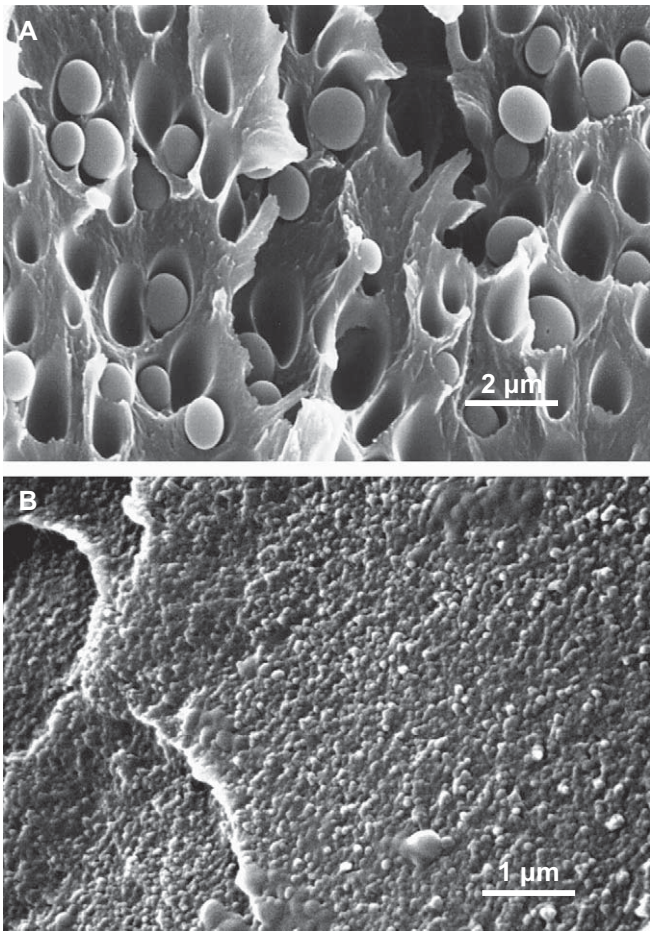

Fig. 17. SEM micrographs of the cryogenically fractured surfaces of: (A) microcomposite with 22.3 wt% of silica; (B) nanocomposite with 22.3 wt% of silica.

two-phase structure much more effective in reducing the molecular motions of the polyimide chains.

4. Conclusions

The molecular structure of the silica phase in polyimide/silica hybrids obtained via the sol–gel route is strongly dependent on the presence of the GOTMS coupling agent. In fact, GOTMS induces the formation of linear, branched chains which render the inorganic phase poorly interconnected. The same occurs in the pure inorganic system, which indicates that the sol–gel chemistry is not affected by the presence of the polyimide precursor and its solvents. The strong influence of GOTMS on the final morphology of the hybrid system should therefore be related to the phase separation mechanism, and, more specifically, to a reduction of the rate of particle-growth.

It has been demonstrated that the carbonyl groups of the imide units are capable to form molecular interactions with water molecules which lead to the absorption of up to 2.5 wt% of water. In the hybrid systems the amount of absorbed water increases substantially due to the hydrophilic nature of the inorganic phase. In particular, it is found that the microcomposite absorbs more water than the nanocomposite, possibly due to the presence of macrovoids surrounding the completely detached silica domains. No interactions of the H-bonding type have been detected between the imide carbonyls and the Si–OH groups of the silica phase.

The relaxation processes of the polyimide have been found to be strongly influenced by the presence of the inorganic phase when an interconnected co-continuous system is realized. Much lower effects are observed in the case of conventional two-phase systems. The lowering of the transition peaks and the increase of activation energies found for the nanocomposite sample were attributed to the molecular scale proximity between the two phases.

References

[1] Mascia L. Trends Polym Sci 1995;3:61.
[2] Morikawa A, Iyoku Y, Kakimoto M, Imal Y. Polym J 1992;24:107.
[3] Nandi M, Conklin JA, Salvati Jr L, Sen A. Chem Mater 1991;3:201.
[4] Kioul A, Mascia L. J Non-Cryst Solids 1994;175:169.
[5] Strawbridge I. In: Paul A, editor. Chemistry of glasses. Chapman and Hall; 1990.
[6] Huang H, Glaser RH, Wilkes GL. In: Zeldin M, Winne KJ, Allcock HR, editors. Inorganic and organometallic polymers. ACS symposium series, vol. 360. Washington, DC: ACS; 1987.
[7] Musto P, Ragosta G, Scarinzi G, Mascia L. Polymer 2004;45:1697.
[8] Musto P, Ragosta G, Scarinzi G, Mascia L. Polymer 2004;45:4265.
[9] Gosh MK, Mittal KL. Polyimides; fundamentals and applications. New York: Marcel Dekker; 1996.
[10] Feger C. Polyimides: trends in materials and applications. New York: Society of Plastic Engineers; 1996.
[11] Bessonov MI, Zubkov VA. Polyamic acids and polyimides: synthesis, transformation and structure. Boca Raton: CRC Press; 1993.
[12] Thompson LF, Willson CG, Tagawa S. Polymers for microelectronics: resists and dielectrics. In: ACS symposium series, vol. 537. Washington, DC: ACS; 1994.
[13] Ikeda RM. J Polym Sci Polym Lett Ed 1966;4:353.
[14] Bernier GA, Kline DE. J Appl Polym Sci 1968;12:593.
[15] Gillham JK, Hallock KD, Stanknicki SJ. J Appl Polym Sci 1972; 16:2595.
[16] Kochi M, Shimada H, Kambe H. J Polym Sci Polym Phys Ed 1984; 22:1979.
[17] Arnold FE, Bruno KR, Shen D, Eashoo M, Lee CJ, Harris FW, et al. Polym Eng Sci 1993;33:1373.
[18] Bessonov MI, Kuznetsov NP, Adrova NA, Florinskij FS. Vysokomol Soedin 1974;A16:2093.
[19] Lushcheikin GA, Gringut BS. Vysokomol Soedin 1974;B14:53.
[20] Adrova NA, Borisova TI, Nikonorova NA. Vysokomol Soedin 1974; B16:621.
[21] Lushcheikin GA, Surova VV, Vorob'yov VD, Dobrokhotova ML, Emel'yanova LI, Shkurova EG. Vysokomol Soedin 1975;B17:159.
[22] Voishchev VS, Burtseva TA, Voishcheva OV, Valetskij PM, Korshak VV. Vysokomol Soedin 1976;B18:912.
[23] Butta E, de Petris S, Pasquon M. J Appl Polym Sci 1969;13:1073.
[24] Mitchenko YV, Dolgov AV, Krasnov EP. Vysokomol Soedin 1975; A17:2091.
[25] Krasonov EP, Stepan'yan AE, Mitchenko YV, Tolkachev YA, Lukasheva VN. Vysokomol Soedin 1977;A19:1566.
[26] Cotugno S, Larobina D, Mensitieri G, Musto P, Ragosta G. Polymer 2001;42:6431.
[27] Allinger NL. J Am Chem Soc 1977;99:8127.
[28] Galeener FL, Lucovsky G. Phys Rev Lett 1976;37:1474.
[29] Galeener FL. Phys Rev B 1979;19:4292.
[30] Farmer VC, Russel JD. Spectrochim Acta 1964;20:1149.

[31] Mauritz KA, Warren RM. Macromolecules 1989;22:1730.
[32] Colthup NB, Daly LH, Wiberley SE. Introduction to infrared and Raman spectroscopy. New York: Academic Press; 1990.
[33] Bellamy LJ. The infrared spectra of complex molecules. New York: Chapman and Hall; 1975.
[34] Musto P, Lavorgna M, Mensitieri G, Ragosta G. Vibrational spectroscopy investigations on the molecular mechanism of H_2O transport in polyimide and polyimide/silica hybrids. Macromolecules, submitted for publication.
[35] Yang DK, Koros WJ, Stannet VT. J Appl Polym Sci 1985;30:1035.
[36] Yang DK, Koros WJ, Hopfenberg HB, Stannet VT. J Appl Polym Sci 1986;22:1619.
[37] Seo J, Han H. J Appl Polym Sci 2001;82:731.
[38] Musto P, Mascia L, Mensitieri G, Ragosta G. Polymer 2005;46:4492.
[39] Yen CT, Chen WC, Liaw DJ, Lu HY. Polymer 2003;44:7079.
[40] Shang XY, Zhu ZK, Yin J, Ma XD. Chem Mater 2002;14:71.
[41] Hasegawa M, Horie K. Prog Polym Sci 2001;26:259.
[42] Kim YH, Moon BS, Harris FW, Cheng SZD. J Therm Anal 1996;46:921.
[43] Li FM, Fang S, Ge JJ, Chen PS, Harris FW, Cheng SZD. Polymer 1996;40:4987.
[44] Qu W, Kao TM, Vora RH, Chung TS. Polymer 2001;42:6393.
[45] Starkweather HWJ. Polymer 1991;32:2443.
[46] Starkweather HWJ. Macromolecules 1990;23:328.